ELSEVIER

Nuclear Physics A 579 (1994) 173–196

NUCLEAR PHYSICS A

Effective interactions for $A = 41$–66 nuclei

M.G. van der Merwe [a], W.A. Richter [a], B.A. Brown [b]

[a] *Physics Department, University of Stellenbosch, Stellenbosch 7600, South Africa*

[b] *National Superconducting Cyclotron Laboratory, and Department of Physics and Astronomy, Michigan State University, East Lansing, MI 48824, USA*

Received 7 December 1993; revised 14 June 1994

Abstract

A new two-body interaction is derived for nuclei in a large part of the 0f1p shell by fitting two-body matrix elements to 494 energy levels in $A = 41$–66 nuclei. For the shell-model basis a ^{40}Ca core and a model space consisting of $0f_{7/2}^{n}(1p_{3/2}0f_{5/2}1p_{1/2})^{m} + 0f_{7/2}^{n-1}(1p_{3/2}0f_{5/2}1p_{1/2})^{1+m}$ configurations was assumed. By varying 40 linear combinations of matrix elements and fixing those that are not well-determined to values of a previously determined starting interaction, an r.m.s deviation between fitted and experimental energies of 193 keV has been achieved. An excellent reproduction of low-lying energy levels, and the magnetic dipole and electric quadrupole moments for the ground states as well as some excited states, is obtained with the new interaction. Further calculations with the new interaction also suggest that it is a valuable extension to the region of nuclei far from stability and to the mass regions currently of astrophysical interest.

1. Introduction

New two-body interactions were recently derived for nuclei in the lower part of the 0f1p shell [1] by considering the complete set of basis states which can be generated from the four orbits $0f_{7/2}$, $1p_{3/2}$, $0f_{5/2}$, $1p_{1/2}$. These effective interactions were systematically derived by fitting: (i) a semi-empirical interaction to 61 energy data from 12 nuclei in the mass range 41 to 49 and (ii) two-body matrix elements (TBME) to the same 61 energy data using the linear combination (LC) method. In order to extend this study to a higher mass range in the fp shell one must truncate the model space, because the rapid increase of the dimensions of the basis states with mass number cannot be handled by available computing capabilities. Monte Carlo methods recently applied to the nuclear shell model [2] allowed full fp-shell calculations, but its scope is limited to the lowest state of each spin and to moments of transition operators.

SSDI 0375-9474(94)00315-E

Van Hees and Glaudemans [3] carried out extensive shell-model calculations on nuclei for $A = 52$–55 by using a model space that allowed for the excitation of only one $f_{7/2}$ nucleon to the $p_{3/2}$, $f_{5/2}$ and $p_{1/2}$ orbits, i.e. $0f_{7/2}^{n} + 0f_{7/2}^{n-1}(1p_{3/2}0f_{5/2}1p_{1/2})^{1}$. We will refer to this model space as the FPV model space. The eight $(f_{7/2})^2$ TBME were determined from fits to energy data and the remaining 52 TBME were taken equal to a modified Kuo–Brown interaction. They found that observables calculated in this model space agreed better with experiment than the values obtained when using a simple $(f_{7/2})^n$ model space. Shell-model calculations were also carried out by Koops and Glaudemans [4] for Ni and Cu isotopes up to masses 67 and 68, respectively, using an MSDI interaction in an unrestricted $(1p_{3/2}, 0f_{5/2}, 1p_{1/2})$ shell-model space.

A hybrid interaction, which is based on a combination of the interactions of Van Hees and Glaudemans and Koops and Glaudemans (we will refer to it as the FPV interaction), generally produces reasonable results for the fp shell [5]. However, the FPV interaction applied in the FPV model space produces too little binding for the ground states of nuclei in general and this shortcoming becomes a major factor higher up in the shell (typically for $A \geqslant 49$) where the discrepancy often amounts to several MeV. To improve on the FPV interaction, we initially adopted the FPV model space that allowed for the excitation of only one particle to the $1p_{3/2}$, $0f_{5/2}$, $1p_{1/2}$ subshells, i.e. $0f_{7/2}^{n} + 0f_{7/2}^{n-1}(1p_{3/2}0f_{5/2}1p_{1/2})^{1}$. By using this model space 401 Coulomb-corrected binding and excitation energies in the mass range $A = 41$–57 could be fitted to semi-empirical interaction forms and two-body matrix elements using similar methods employed for the full fp shell. In addition to a mass dependence for the two-body matrix elements, a mass dependence for the single-particle energies was also employed. By varying only a small number of parameters (15 for the potential model and 25 for the TBME fits), r.m.s deviations between fitted and experimental energies of about 250 keV were achieved. The interactions are called POT5 and TBME5 to reflect their origin, where the numeral is the iteration number. The resulting wave functions were used extensively to calculate various spectroscopic quantities, leading to excellent results [5].

However, a major shortcoming of that study was the severe restriction applied to the occupation of particles in the $(1p_{3/2}, 0f_{5/2}, 1p_{1/2})$ subshells. As a further step we therefore investigated the same methods of extracting an interaction in a model space incorporating 1p–1h excitations from the $0f_{7/2}$ shell with $0f_{7/2}^{n}(1p_{3/2}0f_{5/2}1p_{1/2})^{m} + 0f_{7/2}^{n-1}(1p_{3/2}0f_{5/2}1p_{1/2})^{1+m}$ configurations, where m is the minimum number of nucleons outside the $0f_{7/2}$ subshell. Nuclei in the mass region $A = 41$–66 and approximately 500 energy levels could be included in this study. Problems associated with the convergence of the interaction when a semi-empirical potential was used led to its abandonment in favour of the two-body matrix element fits. An r.m.s. deviation between experiment and theory of 193 keV was achieved for the final fit, in which 40 parameters in total were varied. It was also found necessary to incorporate a mass dependence for both the single-particle energies and the two-body matrix elements in the fits. The new effective interaction derived in this study should prove to be useful for the description of nuclei up to $A = 66$ in the 0f1p shell. It can also be seen as a valuable extension to mass

regions far from stability as well as mass regions that are currently of astrophysical interest.

Although various calculations of shell-model wave functions in the lower part of the fp shell have been carried out in the past (see, for example, the references listed in Ref. [1]), these have not been applied to such an extensive mass range as the present study. The shell-model calculations have been carried out on a VAX 785 computer and more recently on a VAX 6000-410, at Stellenbosch University using the shell-model code OXBASH [6]. The energies of the selected states were calculated relative to a ^{40}Ca core. A correction for the Coulomb energies of the valence protons was applied to the experimental binding energies relative to ^{40}Ca. The Coulomb energies were estimated from the difference in binding energies between pairs of analog states, one of the states generally being a ground state. The uncertainties in the Coulomb corrections are small compared to the energy fit deviations (see also Ref. [7]). In cases where the binding energies between pairs of analog states were not known, the Coulomb energies were estimated from extrapolations of experimental displacement energy systematics. The Coulomb corrections used for the fits are given in Table 1. These values are very close to the set calculated by Cole making use of a semi-empirical formula [8].

The technique of applying a spin–tensor decomposition to the two-body matrix elements of an interaction (see Refs. [9,10]) plays a central role in our analysis of effective interactions. At various stages of our calculations the interactions derived were subjected to a spin–tensor decomposition to monitor the changes in the different interaction components and to compare their values with realistic interactions.

In Section 2 the two different methods considered in the current study to obtain effective interactions are discussed. The form assumed for the semi-empirical interaction is discussed in Subsection 2.1. Due to the problems encountered in obtaining a reliable effective interaction for the mass range under study with the semi-empirical method (see Subsection 2.1), this method was abandoned in favour of the linear combination (LC) method. The rest of the study therefore concentrated on the linear combination method. In Subsection 2.2 the interaction obtained with the use of the LC-method is briefly reviewed. The selection of data and results of the fits are discussed in Section 3. Various results based on the new interaction are presented in Section 4. The theoretical energies calculated with the interaction are compared with experiment in Subsection 4.1, and in Subsection 4.2 the spin–tensor decomposition of the interaction is discussed.

The wave functions obtained from the new interaction were used to calculate some spectroscopic quantities. In Subsection 4.3 the calculated magnetic dipole and electric quadrupole moments for ground states as well as low-lying excited states of the nuclei under consideration, are compared with experimental values.

2. The effective interaction

In Ref. [11] a semi-empirical interaction based on one-boson exchange potentials (OBEP) plus core-polarization correction terms of the multipole-multipole type, was

Table 1
Coulomb corrections (ΔE_C) to experimental binding energies

Nucleus	ΔE_C (MeV)	Nucleus	ΔE_C (MeV)
^{42}Sc	7.214	^{50}V	22.396
^{43}Sc	7.242	^{50}Cr	30.564
^{44}Sc	7.222	^{51}Ti	14.556
^{44}Ti	14.811	^{51}V	22.319
^{45}Sc	7.216	^{51}Cr	30.456
^{45}Ti	14.778	^{51}Mn	38.892
^{46}Sc	7.173	^{52}V	22.260
^{46}Ti	14.758	^{52}Cr	30.344
^{47}Sc	7.191	^{52}Mn	38.756
^{47}Ti	14.719	^{52}Fe	47.574
^{47}V	22.555	^{53}Cr	30.25
^{48}Sc	7.175	^{53}Mn	38.59
^{48}Ti	14.693	^{53}Fe	47.37
^{48}V	22.507	^{54}Mn	38.44
^{48}Cr	30.734	^{54}Fe	47.17
^{49}Sc	7.085	^{55}Fe	46.98
^{49}Ti	14.591	^{55}Co	55.96
^{49}V	22.409	^{56}Co	55.69
^{49}Cr	30.579	^{56}Ni	65.15
^{50}Sc	7.134	^{57}Ni	64.87
^{50}Ti	14.597		

systematically developed by carrying out numerous least-squares fits to the same basic sd-shell data set used by Wildenthal [12] in fitting two-body matrix elements. For the 0f1p shell the same interaction form has been adopted by Richter et al. [1]. Other refinements to the interaction used in Ref. [11], such as the inclusion of a density dependence and a mass dependence of the two-body matrix elements, were also employed by Richter et al. [1], who referred to this interaction form as a modified surface one-boson-exchange potential (MSOBEP).

The development of an empirical interaction based on the linear combination (LC) method was also considered in the study of Richter et al. [1]. Since essentially the same interaction models and fitting procedures are used in this study and these are discussed extensively in that paper, the reader may wish to consult Ref. [1].

2.1. The semi-empirical potential fits

As a starting point we used the same semi-empirical interaction form as used in Ref. [1]. The density dependence of the interaction as well as the mass dependence of the two-body matrix elements (TBME) and single-particle energies (SPE) were

assumed to be of the same form as used in Ref. [5] (see also Subsection 2.2, Eqs. (1) and (2), respectively). However, numerous trials showed that a good reproduction of the experimental data was not possible when only the parameters of the central component of the interaction and the single-particle energies were varied, while the parameters of the tensor and spin–orbit components of the interaction were kept fixed at predetermined values. An interaction form where the parameters for the tensor and spin–orbit components of the interaction were also varied was therefore considered next. (This interaction was very similar in form to the SDPOTA interaction of Brown et al. [11].)

However, a problem arose in that some of the spin–orbit and tensor parameters were abnormally large, a fact borne out when we compared the spin–tensor decomposition plot of our interaction with the interaction of Kuo and Brown (KB) [13]. The values were in general up to three times the value of some of the largest KB values. This problem can probably be attributed to the fact that we used a strongly truncated model space, preventing the spin–orbit and tensor components from being well determined. An enlargement in the model space might help in the elimination of this problem, but this was not possible in this study due to computer limitations. The complication in the determination of the spin–orbit and tensor parameters further seemed to hinder the convergence of the interaction during the iteration process Due to the large amount of computer time involved in the iteration process (about 350 hours CPU time) and the problems mentioned above, we decided to abandon the search for a semi-empirical interaction in the mass range $A = 41$–66 under consideration, in favour of the linear combination (LC) method.

2.2. *The empirical interaction fits*

When fitting two-body matrix elements and single-particle energies in the fp shell to an energy data set, one is faced with the problem that there are a large number of parameters to be determined from the data set. However, the number of parameters can be restricted by a method referred to as the linear combination (LC) method [11,14] (also known as the diagonal correlation matrix method [15]). The least-squares fit problem is reformulated in terms of uncorrelated linear combinations of the one- and two-body matrix elements, or "orthogonal" parameters. The eigenvectors of the error matrix give uncorrelated linear combinations of the parameters and the corresponding eigenvalues give the uncertainties in these linear combinations. The orthogonal parameters can be ordered according to their uncertainty and the well-determined parameters separated from the poorly determined ones. Some constraints are now added to the least-squares fit so that most of the matrix elements are held fixed at values corresponding to some starting interaction, except for those that are well-determined by the data set.

The linear combination (LC) method proved to be successful in obtaining an effective interaction for the mass range $A = 41$–66 under study. The reason why the LC method succeeded, in contrast to the failure of the semi-empirical method, can probably be attributed to the different restrictions placed on the interactions. In the semi-empirical

method all matrix elements are varied in terms of the strength parameters built into the potential form, while in the LC method only a small set of best-determined linear combinations of parameters (matrix elements) are varied, the rest being kept fixed at predetermined values.

2.3. Parameters of the interaction

The success of the method is linked to the choice of the starting interaction to which the poorly determined linear combinations are fixed. In our preliminary work an interaction was derived in the FPV model space (that allowed the excitation of only one particle to the $p_{3/2}$, $f_{5/2}$, $p_{1/2}$ subshells) for $A = 41$–57 nuclei by varying 25 linear combinations of matrix elements. The starting interaction was the FPV interaction, consisting of 60 two-body matrix elements used by van Hees and Glaudemans [3] in the $A = 52$–55 mass range, and the rest were MSDI values used by Koops and Glaudemans [4] for Ni and Cu isotopes in the $A = 57$–68 range. Five iterations were needed, leading at each stage to an interaction TBME*n*, where *n* is the number of the iteration, leading to a final r.m.s. deviation of 250 keV. The interaction TBME4, which was used to calculate the final one-body and two-body transition densities, is used as the starting interaction in the present work.

It was found that in order to get a good reproduction of the single-particle energies (SPE) of ^{41}Ca and to get a good fit in general, the single-particle energies must also be mass dependent, in contrast to the assumption in the sd shell [11] and the full fp shell [1], but similar to the assumption in the truncated fp-shell study [5]. A simple linear mass dependence of the form

$$\mathrm{SPE}(A) = \mathrm{SPE}(A=41) + \frac{A-41}{66-41}[\mathrm{SPE}(A=66) - \mathrm{SPE}(A=41)] \qquad (1)$$

was used for each of the four single-particle energies ($0f_{7/2}$,$1p_{3/2}$,$0f_{5/2}$ and $1p_{1/2}$). These "$A = 66$" SPE represent the kinetic energy plus the interaction of the nucleons in the fp shell with those in the 0s, 0p and 1s0d closed shells. The total binding energies of the $A = 66$ nuclei are obtained from these "$A = 66$" SPE plus the contribution from the interactions between nucleons in the fp shell.

In the present case the interaction is in principle determined by 195 TBME and the 8 SPE parameters. Due to the model space truncation the twenty $\langle f_{7/2}f_{7/2}|V|\gamma_j\delta_j\rangle$ two-body matrix elements, with γ_j and δ_j any of the $p_{3/2}$, $f_{5/2}$ or $p_{1/2}$ shells, are not determined. These are set equal to the FPV interaction. In addition the six $\langle\alpha_j\alpha_j|V|p_{1/2}p_{1/2}\rangle$ two-body matrix elements, with α_j any of the subshells $p_{3/2}$, $f_{5/2}$, $p_{1/2}$, are extremely insensitive to the data set and are also set equal to the FPV interaction. Thus we start with 177 parameters.

The 40 best-determined linear combinations out of this set of 177 parameters were allowed to vary, while the remaining ones were fixed at the TBME4 starting interaction. The mass dependence A^{-p} of the two-body matrix elements was also investigated in the current study. The optimum value used was $p = 0.50$. This is the same value used in

Ref. [5]. The renormalized TBME, after consideration of the assumed mass dependence, will therefore be of the form

$$\langle V\rangle(A) = \langle V\rangle(A/42)^{-0.50}. \tag{2}$$

3. Data selection and results of the fits

Although we originally started off with 541 energy level data, this was reduced to 494 in order to obtain better convergence of the iteration process. The final interaction, henceforth referred to as the TBLC8 interaction, was obtained by fitting to the set of 494 Coulomb-corrected energy data. In order to obtain a reasonable convergence of the interaction, five iterations were required. It should be mentioned that because of the considerable computation time required another iteration was not attempted. As a result the fitted energy values differ in most cases from the values calculated with the interaction by a few tens of keV, with deviations in the mass 58 to 60 region reaching values of about 100 keV.

The data set of 494 energy levels span 74 nuclei in the mass range A = 41–66. Care was taken to exclude intruder states, i.e. states with significant admixtures of configurations lying outside the adopted model space, as far as possible. (See also the discussion in Ref. [1].)

The weighting of the experimental data used corresponded to adding a theoretical error of 150 keV in quadrature to the experimental error. The normalized χ-value for the "best-fit" empirical interaction in the sd shell [11] with the same weighting was about 1.0, and in the present case it was 1.334.

In our model space ^{41}Ca can have only four single-particle levels, whereas more than 40 levels have been observed below 5 MeV excitation. Single-particle stripping to ^{41}Ca suggests that the $f_{7/2}$ strength is almost entirely concentrated in the ground state, the $p_{3/2}$ strength is spread over two states and the $f_{5/2}$ and $p_{1/2}$ strengths over several levels. For each single-particle level the centroid of the observed single-particle energies, weighted by single-nucleon spectroscopic factors, has been used for the experimental value. The experimental values used for the single-particle levels are the same values used by Van Hees and Glaudemans [3] in their calculations.

The final value for the r.m.s. deviation between experimental and fitted energy levels of 193 keV for the 494 levels implies that an excellent overall fit was achieved. The interaction is called TBLC8. Some details will be discussed in the next section. The largest deviations were observed for the odd–odd nuclei ^{58}Co and ^{56}Co. For comparison the spectra for an interaction due to Horie and Ogawa [16,17] and for the the FPV interaction, were calculated for the two nuclei in question. The interaction of Horie and Ogawa (HO) applies to a model space $(0f_{7/2})_p^{Z-20} \times (1p_{3/2}, 0f_{5/2}, 1p_{1/2})_n^r$, with n and p referring to neutrons and protons, respectively, outside a ^{48}Ca core and was obtained from fits to energy spectra for $N = 29$ nuclei.

For ^{58}Co the HO interaction gives for the lowest excited states J, E_{ex} (in MeV): (5, −0.138), (4, −0.132), (3, −0.178), (6, 0.876), the FPV interaction gives (5, 0.175), (4, 0.224), (3, 0.374), (6, 1.409) and the TBLC8 interaction (5, −0.303), (4, −0.328), (3, −0.507) and (6, 0.675). Both are somewhat better than our results. For the lowest few states in ^{56}Co the HO interaction gives J, E_{ex} (in MeV): (3, 0.216), (5, 0.407), (4, 0.839), (2, 0.983), (5, 1.263), (3, 1.138), the FPV interaction gives (3, 0.207), (5, 0.675), (4, 1.276), (2, 1.092), (5, 1.523), (3, 1.577) and the TBLC8 interaction (3, 0.512), (5, 0.388), (4, 1.309), (2, 1.220), (5, 1.296), (3, 1.188). For the few lowest states both interactions are again somewhat better than ours but start to get comparatively much worse for the higher excited states. It is evident from the above that problems with the reproduction of the ^{58}Co and ^{56}Co level schemes persist also for the HO and FPV interactions.

4. Results

4.1. Calculated level spectra

The final TBLC8 interaction gives an excellent reproduction of the experimental energies of the fitted levels. The experimental spectra for the low-lying normal parity

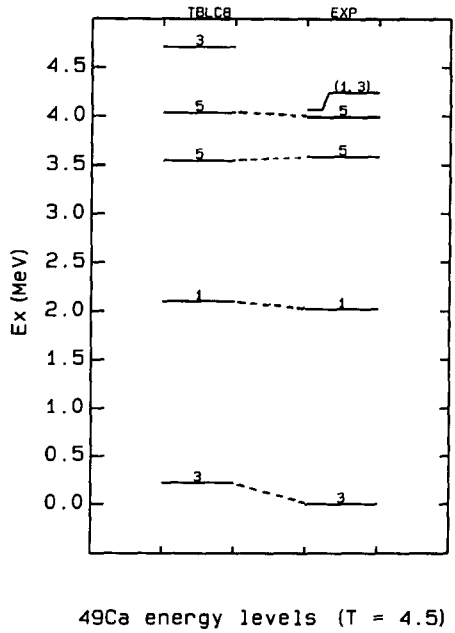

Fig. 1. Comparison of theoretical and experimental energy spectra for low-lying natural parity levels in ^{49}Ca. The experimental spectra are compared with those of the TBLC8 interaction, with the experimental ground-state energy taken as zero. Levels connected by dashed lines were included in the fits. Where available the energy levels obtained with the TBME5 and POT5 interactions of Ref. [5] are also indicated. J is indicated for A even and $2J$ for A odd.

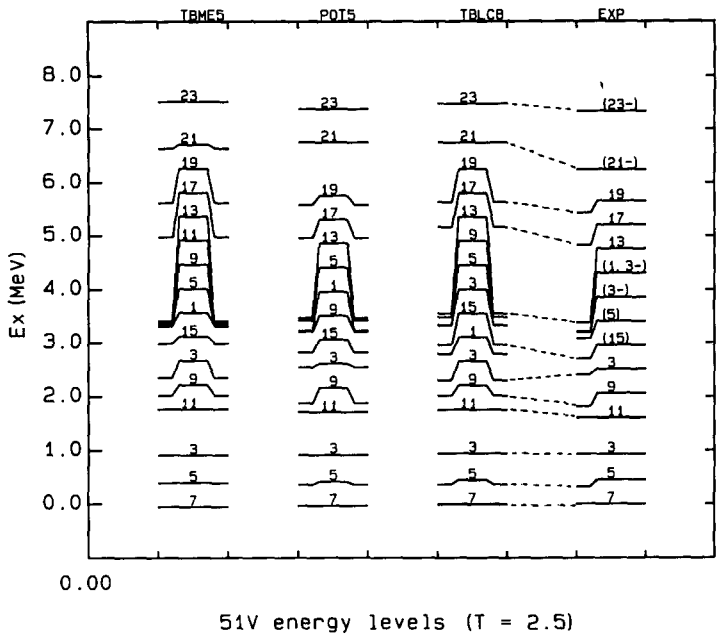

Fig. 2. Energy levels of ^{51}V. Conventions are the same as in Fig. 1.

states are compared with those of the TBLC8 interaction for some representative nuclei in Figs. 1–8. The results are also in certain cases compared with the level spectra obtained from the semi-empirical POT5 and the empirical TBME5 interactions (see Subsections 2.1 and 2.2).

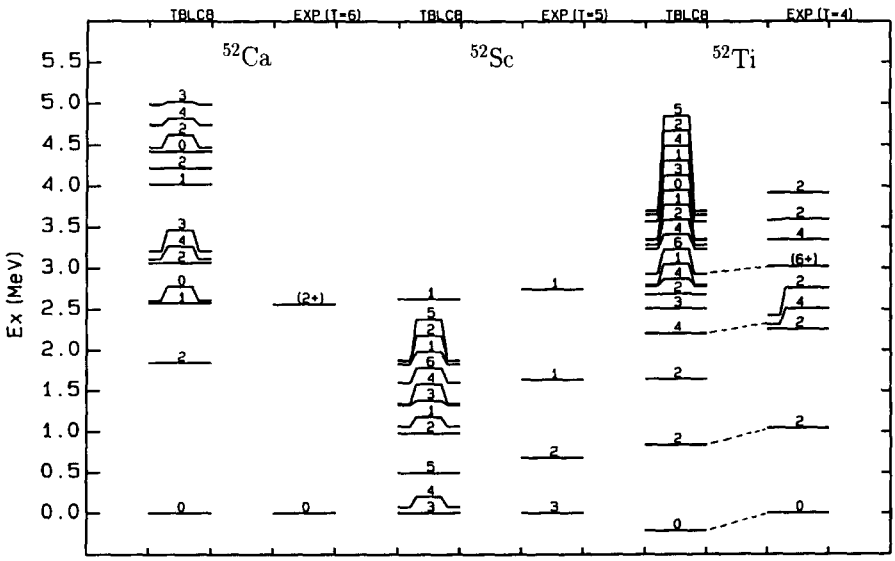

Fig. 3. Energy levels of $A = 52$ nuclei. Conventions are the same as in Fig. 1.

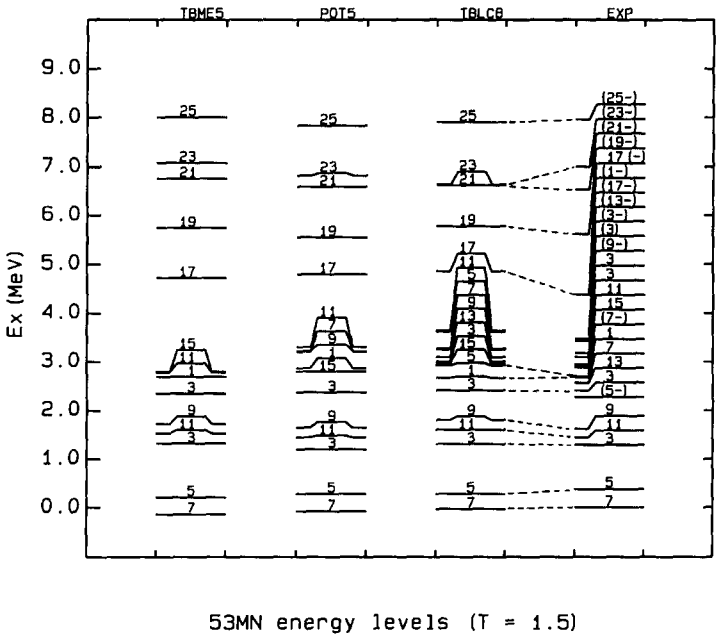

Fig. 4. Energy levels of ^{53}Mn. Conventions are the same as in Fig. 1.

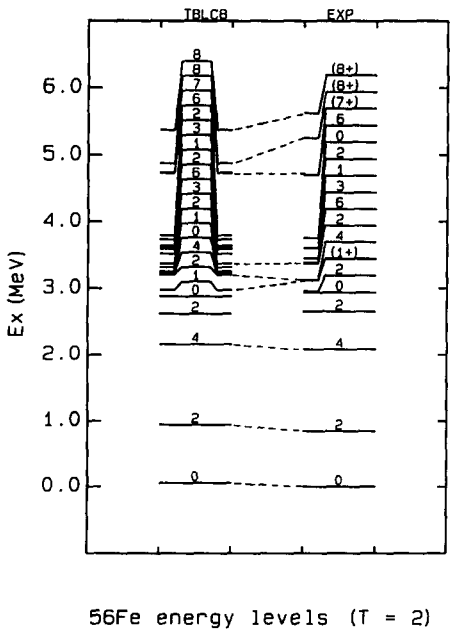

Fig. 5. Energy levels of ^{56}Fe. Conventions are the same as in Fig. 1.

All levels up to the highest level shown, in each case, have been included, except where otherwise indicated. Additional levels not included in the fits are generally also shown for the TBLC8 interaction to indicate where some of the lower-lying levels are predicted to be. Levels connected by dashed lines were those included in the fits.

4.1.1. The spectrum of ^{49}Ca

In ^{49}Ca the three predominant single-particle states, i.e. the $\frac{3}{2}^-$ ground state, the $\frac{1}{2}^-$, 2.023 MeV state, and the $\frac{5}{2}^-$, 3.586 MeV state, are all well reproduced in the TBLC8 spectrum.

4.1.2. The spectrum of ^{51}V

All the energy levels up to the first $\frac{13}{2}^-$ level are shown for TBLC8. After that only the fitted levels are shown. The energy levels are all very well reproduced as far as ordering and spacing of the levels are concerned. Counterparts exist in the TBLC8 calculation for most of the experimentally determined levels.

4.1.3. The spectra of A = 52 nuclei (^{52}Ca, ^{52}Sc and ^{52}Ti)

These three nuclei are of interest in providing a test for shell-model calculations far from the line of stability. Only ^{52}Ti was included in the data set used to obtain the TBLC8 interaction. Huck et al. [18] did an experimental study on the beta decay of the isotopes ^{52}K, ^{52}Ca and ^{52}Sc and also made use of the Kuo–Brown interaction with a few monopole changes to study the daughter nuclei in terms of shell-model calculations in an FPV model space. The TBLC8 interaction reproduces the experimental energy levels of the ^{52}Ca, ^{52}Sc and ^{52}Ti isotopes slightly better than the study of Huck et al. [18].

4.1.4. The spectrum of ^{53}Mn

All the energy levels up to the second $\frac{11}{2}^-$ level are shown for the TBLC8 interaction. After that only the fitted high-spin states are shown. The level ordering and spacing are excellently reproduced with the TBLC8 interaction. The high-spin states are also reproduced well.

4.1.5. The spectrum of ^{56}Fe

For the TBLC8 interaction all the levels up to the second 6^+ level have been included in the figure. After that only the levels used in the fit to experimental data are shown. In ^{56}Fe the correspondence between experiment and the predicted levels is generally very good. The high-spin states are also well produced.

4.1.6. The spectrum of ^{57}Ni

The low-lying levels in ^{57}Ni can be divided into basically two groups; one comprises the lowest three levels with $J = \frac{3}{2}^-$ (ground state), $\frac{5}{2}^-$ (0.77 MeV) and $\frac{1}{2}^-$ (1.112 MeV), which are usually regarded as single-particle states and the other the "core excited" levels observed above the first $J = \frac{7}{2}^-$ level at 2.577 MeV [19]. The

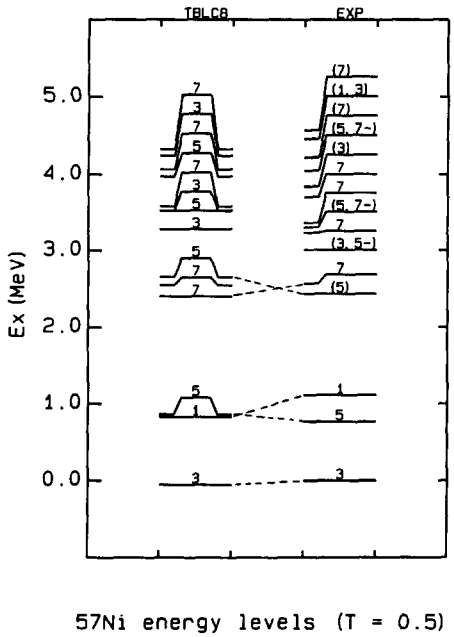

Fig. 6. Energy levels of ^{57}Ni. Conventions are the same as in Fig. 1.

single-particle states are reproduced at approximately the correct position, although there is a reversal in order between the first $\frac{1}{2}^-$ and $\frac{5}{2}^-$ levels as well as the second $\frac{5}{2}^-$ and first $\frac{7}{2}^-$ levels when comparing the TBLC8 spectrum with the experimental spectrum. The first $\frac{7}{2}^-$ level is also reproduced at approximately the right position.

4.1.7. The spectrum of ^{59}Cu

The first four experimental energy levels are all well reproduced in the TBLC8 spectrum.

4.1.8. The spectrum of ^{66}Ni

The level ordering and spacing are reproduced well for the 0^+ ground state as well as the first and second 2^+ and 4^+ states. With the exception of some of the 0^+ states, theoretical counterparts exist for all the low-lying experimental levels. Assuming the indicated experimental assignments, all the 2^+ and 4^+ states are reproduced well in the TBLC8 spectrum.

Spectra obtained for the $N = 29$ and 30 isotones with the TBLC8 interaction are generally better than those obtained in the study of these isotones by Horie and Ogawa [16,17].

In summary, the new TBLC8 interaction generally gives a good account of the low-lying spectra of the $A = 41$–66 nuclei investigated. For the $N = 30$, 31 and 32 nuclei with $A = 52$, the results also support the validity of the model space and the TBLC8 interaction far from stability.

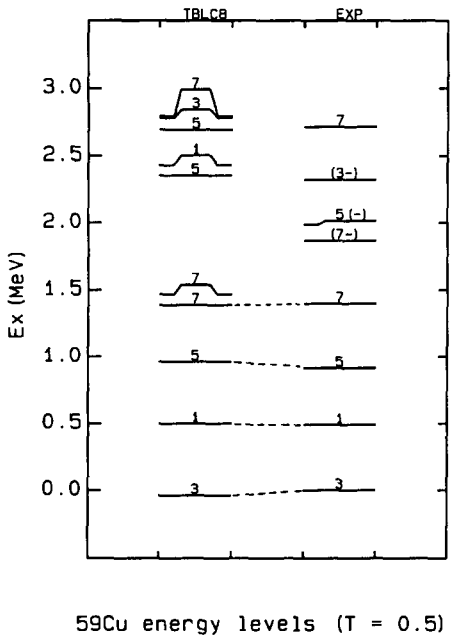

Fig. 7. Energy levels of ^{59}Cu. Conventions are the same as in Fig. 1.

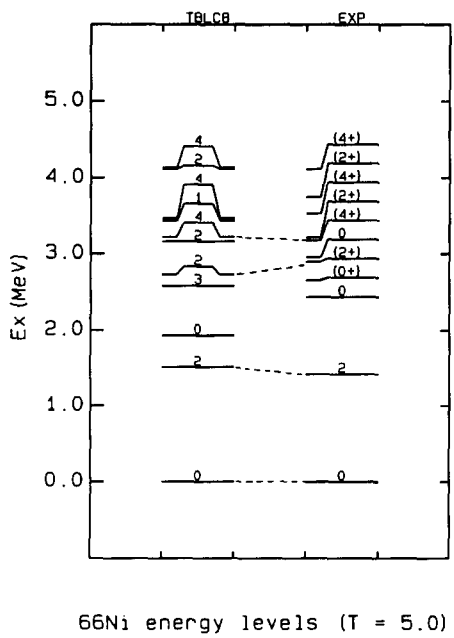

Fig. 8. Energy levels of ^{66}Ni. Conventions are the same as in Fig. 1.

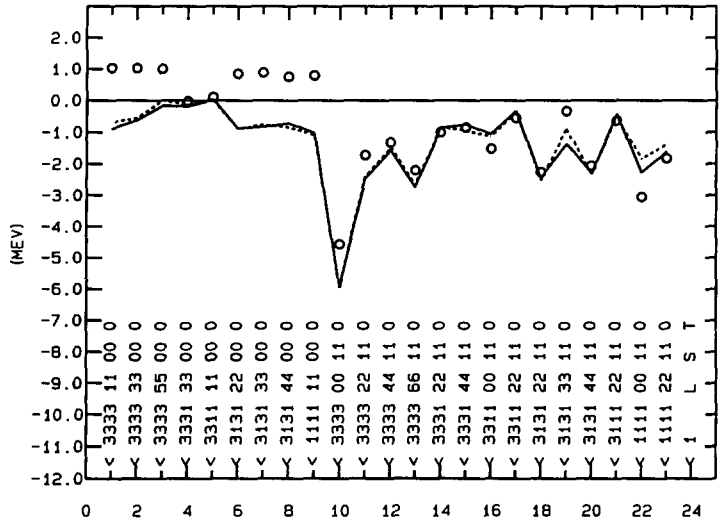

Fig. 9. Matrix elements for the central $T = 0$ component. The TBLC8 (solid line) interaction is compared with the TBME5 (dashed line) interaction of Ref. [5] and the renormalized (circles) Kuo–Brown G-matrices. The labels corresponding to the matrix elements along the horizontal axis are the quantum numbers $l_a l_b l_c l_d LL'SS'T$ in the LS-coupled matrix element $\langle l_a l_b LSJT|V|l_c l_d L'S'JT\rangle$.

4.2. Spin-tensor decomposition

In Figs. 9–16 comparisons are made between the spin-tensor components of the TBLC8 interaction (solid line), the TBME5 (dashed line) interaction [5] and the renormalized (circles) Kuo–Brown G-matrix interaction (KBFP).

In Figs. 9 and 10 the central components of the interactions are compared. The TBLC8 interaction is very similar to the TBME5 interaction, which is not surprising since

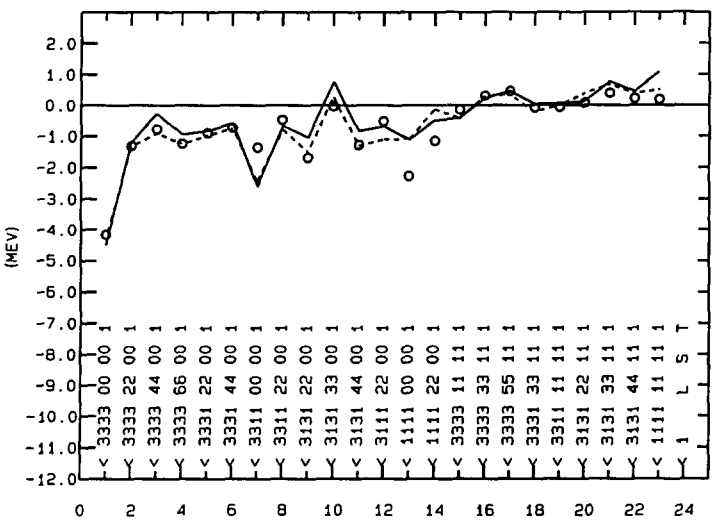

Fig. 10. Matrix elements for the central $T = 1$ component. Conventions are the same as in Fig. 9.

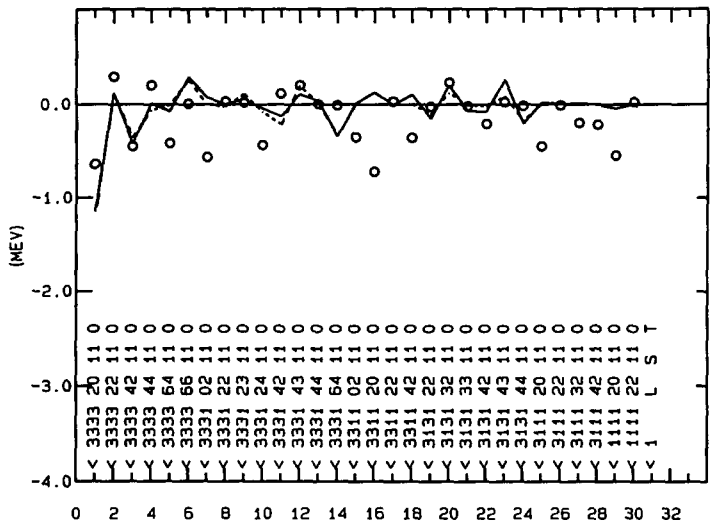

Fig. 11. Matrix elements for the tensor $T = 0$ component. Conventions are the same as in Fig. 9.

TBME5 is equivalent to the starting interaction. The TBLC8 interaction is significantly different from the KBFP interaction, particulary for the $(T, S) = (0, 0)$ channel and since the central components are the most important, this probably accounts for most of the differences obtained with the two interactioons.

In Figs. 11 and 12 the tensor components are compared. The TBLC8 and TBME5 interactions are once again very close to each other. The KBFP matrix elements in the $T = 0$ channel deviate sharply from most other matrix elements, whereas the $T = 1$ matrix elements are generally very small compared to $T = 0$.

For the $T = 0$ spin–orbit components in Fig. 13 the TBLC8 and the TBME5 interac-

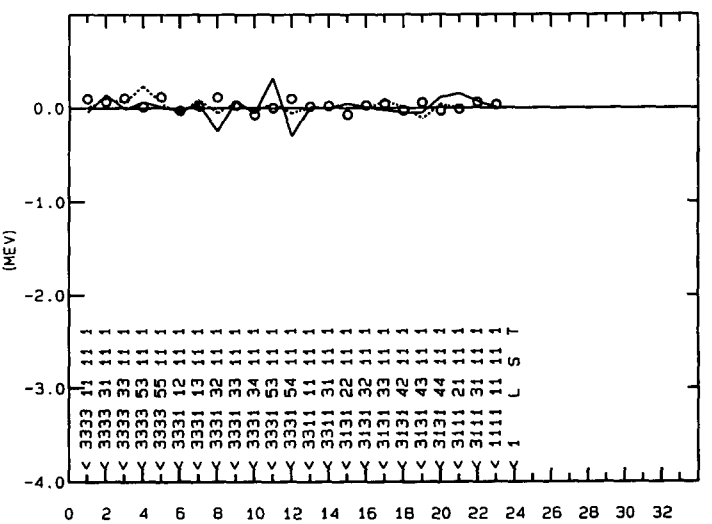

Fig. 12. Matrix elements for the tensor $T = 1$ component. Conventions are the same as in Fig. 9.

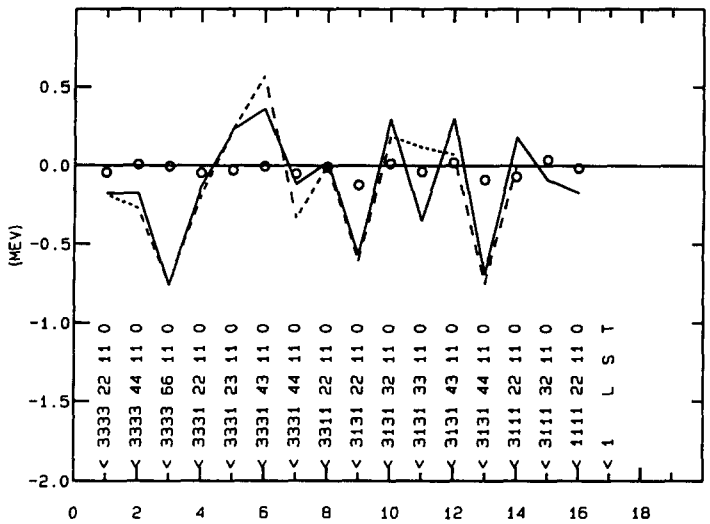

Fig. 13. Matrix elements for the spin-orbit $T = 0$ component. Conventions are the same as in Fig. 9.

tions follow the same general trend, although some deviations do occur. Both interactions deviate sharply from the KBFP interaction, which generally has values about an order of magnitude smaller. For the $T = 1$ case in Fig. 14 the TBLC8 interaction deviates significantly from the other two interactions.

The antisymmetric spin-orbit components are shown in Figs. 15 and 16. The KBFP interaction has very small ALS components, whereas the TBLC8 components have much larger magnitudes (up to about 0.7 MeV), which is often the case for empirical interactions. Of course, it should be kept in mind that the fact that the interaction has been determined in a truncated model space can also affect the different components of

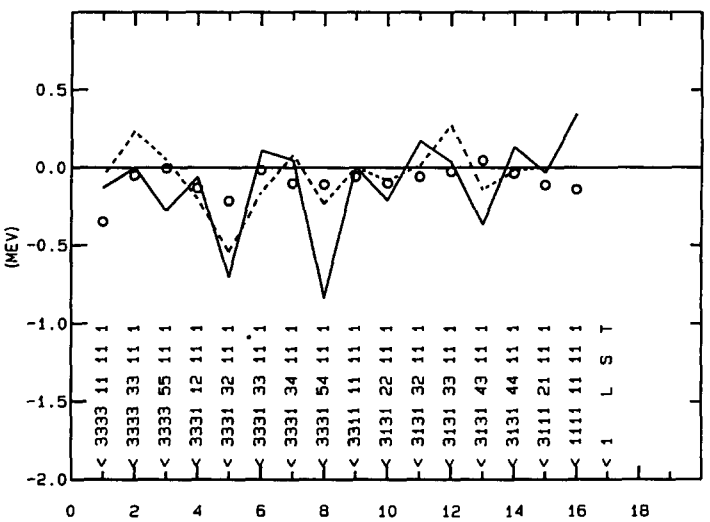

Fig. 14. Matrix elements for the spin-orbit $T = 1$ component. Conventions are the same as in Fig. 9.

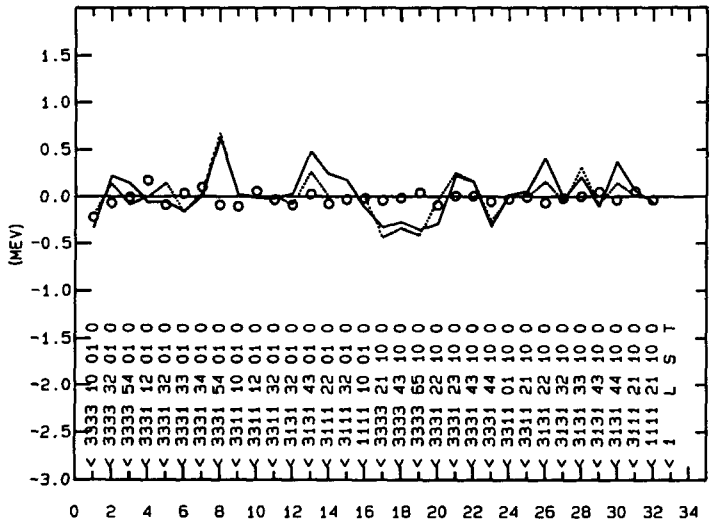

Fig. 15. Matrix elements for the antisymmetric spin–orbit $T = 0$ component. Conventions are the same as in Fig. 9.

the interaction. The TBLC8 interaction components are again close to the values of the TBME5 interaction.

Finally, one of the most significant features of the TBLC8 interaction is the relative enhancement of the spin–orbit and antisymmetric spin–orbit components of the interaction when compared with the KBFP interaction. This may also be due to the truncation used. Also for all important central components it was found that although the TBLC8 interaction follows the same general trend as the KBFP interaction, there are many

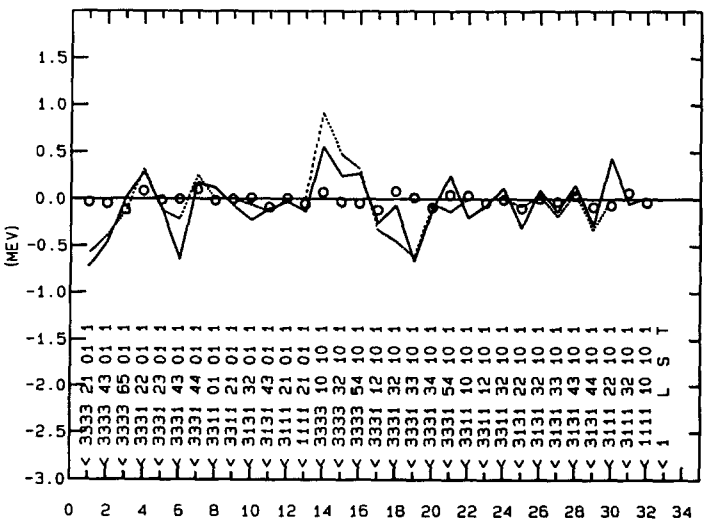

Fig. 16. Matrix elements for the antisymmetric spin–orbit $T = 1$ component. Conventions are the same as in Fig. 9.

differences in detail, e.g. the $(T,S) = (0,0)$ channel. These factors are at the basis of the improved results found for the new interaction.

4.3. Magnetic dipole and electric quadrupole moments

With the wave functions obtained from the TBLC8 interaction, the static electromagnetic moments for nuclei in the mass range considered have been calculated. The calculations used bare g-factors in the first place and secondly effective g-factors (two of the four g-factors were varied) and effective charges to compensate for the configurations excluded by the model space. The optimal values for the effective values were determined by least-squares fits to the experimental data (Table 2).

The calculated magnetic dipole and electric quadrupole moments for the TBLC8 interaction are compared with experimental values in Tables 3 and 4, respectively. The magnetic dipole moments calculated with bare nucleon g-factors are reasonably well reproduced by the new TBLC8 interaction, except for a few notable exceptions, for instance the $\frac{7}{2}^-$ ground state of ^{45}Ti, the $\frac{7}{2}^-$ (0.159 MeV) state of ^{47}Ti, the 2^+ (0.308 MeV) state of ^{48}V, the $\frac{3}{2}^-$ ground state of ^{53}Cr, the $\frac{3}{2}^-$ ground state of ^{57}Ni, the $\frac{5}{2}^-$ (0.339 MeV) state of ^{59}Ni and the $\frac{5}{2}^-$ (0.067 MeV) state of ^{61}Ni. In the other cases, where there is a large discrepancy between the experimental and theoretical values, the experimental error is generally very large. Using fitted effective g^s-proton and g^s-neutron factors specified in Table 2, the agreement for the specific cases mentioned above is improved, except for ^{47}Ti and ^{48}V. Also the overall agreement between experiment and theory is better.

Quadrupole moments have been calculated with effective charges of $e_p = 1.50$ and $e_n = 0.50$ in case I (the values used by Van Hees and Glaudemans [3]), and fitted values of $e_p = 1.486$ and $e_n = 0.840$ for case II. The overall agreement between experimental and theoretical quadrupole moments does not differ much for cases I and II, although calculation II is somewhat better. The theoretical calculated quadrupole moments, Q_{th}^{II}, mostly agree with experiment within the experimental errors. The most notable exceptions are the 2^+ ground state of ^{44}Ca, the $\frac{7}{2}^-$ ground state of ^{45}Ti, the 4^+

Table 2
Values for the g-factors and effective charges

	Bare nucleon value	Effective nucleon value [a]	Effective nucleon value [b]
g^s-proton	5.586	5.031	
g^s-neutron	−3.826	−3.041	
g^l-proton	1.000	1.000	
g^l-neutron	0.000	0.000	
e-proton	1.000	1.486	1.500
e-neutron	0.000	0.840	0.500

[a] Effective values were obtained for g^s-proton and g^s-neutron only by a fit to experimental values.

[b] Values used by Van Hees et al. [3].

Table 3
Comparison of magnetic dipole moments μ (in units of μ_N) for the TBLC8 interaction with experiment. Free nucleon g-factors are used to determine μ_{th}^{free} while the effective nucleon g-factors used for μ_{th}^{eff} are $g_p^s = 5.031$, $g_n^s = -3.041$, $g_p^l = 1.000$, $g_n^l = 0.000$. Experimental values are from Ref. [20] unless stated otherwise; the experimental error in the last significant digit(s) is indicated in parentheses. Absence of a sign at the experimental values means the sign has not been determined by the experiment. E_x is the experimental excitation energy in MeV

Nuclide	$2J$	$2T$	E_x (Mev)	μ_{exp}	μ_{th}^{free}	μ_{th}^{eff}
^{41}Ca	7	1	0.000	−1.594781(9)	−1.913	−1.520
^{41}Sc	7	1	0.000	5.5350(36)	5.793	5.515
^{42}Ca	12	2	3.189	−2.49(9)	−3.084	−2.451
^{43}Ca	7	3	0.000	−1.317643(7)	−1.712	−1.408
^{43}Sc	7	1	0.000	+4.62(4)	4.895	4.687
	19	1	3.123	+3.122(7)	2.855	3.181
^{44}Ca	4	4	1.157	−0.56(22)	−0.9060	−0.7201
^{44}Sc	4	2	0.000	+2.56(3)	2.622	2.532
	8	2	0.350	+3.61(48)	3.031	3.001
	12	2	0.271	+3.88(1)	3.813	3.831
^{45}Ca	7	5	0.000	−1.3274(14)	−1.657	−1.317
^{45}Sc	7	3	0.000	+4.7564866(18)	4.915	4.728
^{45}Ti	7	1	0.000	0.095(2)	−0.2518	−0.03903
	5	1	0.040	−0.133(10)	−0.4151	−0.2769
^{46}Sc	8	4	0.000	+3.03(2)	2.959	2.974
^{46}Ti	4	2	0.889	+0.98(24)	0.9332	0.9661
^{46}V	6	0	0.802	+1.638(30)	1.738	1.810
^{47}Ca	7	7	0.000	−1.380(24)	−1.591	−1.264
^{47}Sc	7	5	0.000	+5.34(2)	5.116	4.919
^{47}Ti	5	3	0.000	−0.78848	−0.8580	−0.6307
	7	3	0.159	−1.93(60)	−0.8145	−0.5426
^{47}V	3	1	0.000		2.351	2.242
^{48}Sc	12	6	0.000		3.439	3.511
^{48}Ti	4	4	0.984	+0.86(38)	0.8101	0.8438
^{48}V	8	2	0.000	2.012(11)	2.247	2.313
	4	2	0.308	+0.444(16)	0.8346	0.8944
^{49}Ca	3	9	0.000		−1.722	−1.368
^{49}Sc	7	7	0.000		5.342	5.135
^{49}Ti	7	5	0.000	−1.10417(1)	−1.248	−0.9433
^{49}V	7	3	0.000	4.47(5)	4.654	4.492
	3	3	0.153	+2.37(12)	2.575	2.459
^{49}Cr	5	1	0.000	0.476(3)	−0.4813	−0.2871
^{50}Sc	10	8	0.000		3.697	3.817
^{50}Ti	4	6	1.554	2.68(84)	2.899	2.786
	12	6	3.199	+9.26(102)	8.742	8.432
^{50}V	12	4	0.000	+3.3456889(14)	3.368	3.455
^{50}Cr	4	2	0.783	+1.18(20)	1.264	1.266
^{51}Ca	3	11	0.000		−0.6916	−0.5497
^{51}Sc	7	9	0.000		5.149	4.966
^{51}Ti	3	7	0.000		−1.556	−1.219
^{51}V	7	5	0.000	+5.14870573(18)	5.226	5.031
	5	5	0.320	+3.68(33)	3.688	3.553
^{51}Cr	7	3	0.000	(−)0.934(5)	−0.9509	−0.6700
^{51}Mn	5	1	0.000	3.5683(13)	3.758	3.601

Table 3 — continued

Nuclide	$2J$	$2T$	E_x (Mev)	μ_{exp}	μ_{th}^{free}	μ_{th}^{eff}
^{52}Sc	6	10	0.000		3.569	3.613
^{52}V	6	6	0.000		2.986	3.066
^{52}Cr	4	4	1.434	+3.00(50)	2.696	2.612
^{52}Mn	12	2	0.000	+3.0622(12)	3.138	3.247
^{53}V	7	7	0.000		4.861	4.695
^{53}Cr	3	5	0.000	−0.47454(3)	−1.357	−1.0330
	7	5	1.289	+2.8(49)	1.476	1.712
^{53}Mn	7	3	0.000	5.024(7)	5.119	4.935
	5	3	0.378	+3.25(30)	3.800	3.652
^{53}Fe	7	1	0.000		−0.7041	−0.4457
^{54}Cr	4	6	0.835	+1.12(20)	1.130	1.132
^{54}Mn	6	4	0.000	+3.2819(13)	2.830	2.874
^{54}Fe	4	2	1.408	+2.16(38)	2.429	2.375
	12	2	2.950	8.22(18)	8.640	8.331
^{55}Mn	5	5	0.000	+3.4687190(9)	3.660	3.510
^{55}Fe	3	3	0.000		−1.283	−0.9636
	5	3	0.931	+2.7(12)	1.760	1.533
	7	3	1.317	+2.0(2.0)	1.028	1.302
^{55}Co	7	1	0.000	+4.822(3)	5.045	4.870
^{56}Fe	4	4	0.847	1.22(16)	1.033	1.039
^{56}Co	8	2	0.000	3.851(12)	3.431	3.510
^{57}Co	7	3	0.000	+4.720(10)	4.854	4.690
	3	3	1.378	+3.0(6)	3.268	3.008
^{57}Ni	3	1	0.000	0.88(6)	−1.606	−1.274
^{58}Co	4	4	0.000	+4.044(8)	4.889	4.602
	8	4	0.053	+4.194(8)	3.591	3.570
	6	4	0.111	+2.22(39)	4.147	4.002
^{58}Ni	4	2	1.454	−0.12(24)	−0.3556	−0.2709
^{58}Cu	2	0	0.000		0.6546	0.7014
^{59}Ni	3	3	0.000		−1.383	−1.0946
	5	3	0.339	+0.35(15)	1.089	0.8819
^{59}Cu	3	1	0.000		2.483	2.308
^{60}Ni	4	4	1.332	+0.18(24)	−0.1499	−0.1042
^{60}Cu	4	2	0.000	+1.219(3)	2.014	1.850
^{61}Ni	3	5	0.000	−0.75002(4)	−1.124	−0.8864
	5	5	0.067	+0.480(6)	1.043	0.8424
^{62}Ni	4	6	1.173	+0.68(14)	0.5953	0.4994
^{63}Ni	1	7	0.000		0.6523	0.5190
	5	7	0.087	+0.752(3)	1.380	1.108
^{65}Ni	5	9	0.000	0.69(6)	1.450	1.162

ground state of ^{46}Sc, the $\frac{7}{2}^-$ ground state of ^{47}Ca, the 2^+ ground state of ^{48}Ti and the $\frac{3}{2}^-$ ground state of ^{61}Ni.

Table 4
Comparison of calculated electric quadrupole moments Q (in units of $e \cdot \mathrm{fm}^2$) with experiment. Effective charges of $e_p = 1.500$ and $e_n = 0.500$ have been used in case I, and $e_p = 1.486$ and $e_n = 0.840$ for case II. Experimental values are from Ref. [20] unless stated otherwise; the experimental error in the last significant digit(s) is indicated in parentheses. Absence of a sign for the experimental values means the sign has not been determined by experiment. E_x is the experimental excitation energy in MeV

Nuclide	$2J$	$2T$	E_x (Mev)	Q_{exp}	Q^{I}_{th}	Q^{II}_{th}
^{41}Ca	7	1	0.000	−8.0(8)	−5.681	−9.545
^{41}Sc	7	1	0.000	−16.6(8) [a]	−17.04	−16.88
^{42}Ca	12	2	1.525		−6.828	−11.47
^{43}Ca	7	3	0.000	−4.9(5)	−2.076	−3.487
^{43}Sc	7	1	0.000	−26(6)	−18.82	−23.00
	19	1	3.123	19.9(14)	−24.36	−29.02
^{44}Ca	4	4	1.157	−14(7)	−3.337	−5.606
^{44}Sc	4	2	0.000	+10(5)	4.283	5.454
	8	2	0.350		−7.200	−9.577
	12	2	0.271	−19(2)	−20.44	−26.48
^{45}Ca	7	5	0.000	+4.6(14)	2.143	3.600
^{45}Sc	7	3	0.000	−22(1)	−20.90	−25.50
^{45}Ti	7	1	0.000	1.5(15)	−4.212	−6.038
	5	1	0.040		−15.07	−18.08
^{46}Sc	8	4	0.000	+11.9(6)	0.4000	2.463
^{46}V	6	0	0.802		23.94	27.85
^{47}Ca	7	7	0.000	+2.1(4)	7.469	12.55
^{47}Sc	7	5	0.000	−22(3)	−21.46	−25.39
^{47}Ti	5	3	0.000	+29(1)	17.31	22.32
	7	3	0.159		8.242	9.380
^{47}V	3	1	0.000		16.78	19.34
^{48}Sc	12	6	0.000		−5.342	−2.870
^{48}Ti	4	4	0.984	−17.7(8)	−6.997	−9.917
^{48}V	8	2	0.000		31.33	36.36
	4	2	0.308		−6.214	−6.865
^{49}Ca	3	9	0.000		−3.687	−6.194
^{49}Sc	7	7	0.000		−19.42	−20.84
^{49}Ti	7	5	0.000	+24(1)	21.56	26.79
^{49}V	7	3	0.000		−9.400	−11.58
	3	3	0.153		16.83	18.91
^{49}Cr	5	1	0.000		27.91	32.76
^{50}Sc	10	8	0.000		−22.92	−26.57
^{50}Ti	4	6	1.554	+8(16)	8.114	8.862
	12	6	3.198		−23.21	−24.50
^{50}V	12	4	0.000	+21(4)	18.02	21.88
^{50}Cr	4	2	0.783	−36(7)	−20.80	−24.36
^{51}Ca	3	11	0.000		4.684	7.869
^{51}Sc	7	9	0.000		−21.83	−25.31
^{51}Ti	3	7	0.000		−8.497	−11.08
^{51}V	7	5	0.000	−5.2(10)	−6.849	−6.978
				−3.3(10		
	5	5	0.320		−14.75	−15.65
^{51}Cr	7	3	0.000		32.41	37.29
^{51}Mn	5	1	0.000	42(7)	29.69	33.98

Table 4 — continued

Nuclide	$2J$	$2T$	E_x (Mev)	Q_{exp}	Q_{th}^{I}	Q_{th}^{II}
^{52}Sc	6	10	0.000		−16.95	−21.00
^{52}V	6	6	0.000		4.337	5.579
^{52}Cr	4	4	1.434	−8.2(16)	−9.158	−9.376
^{52}Mn	12	2	0.000	+50(7)	47.06	52.16
^{53}V	7	7	0.000		−8.980	−11.15
^{53}Cr	3	5	0.000	−15(5)	−12.10	−14.63
	7	5	1.289		−18.75	−21.15
^{53}Mn	7	3	0.000		7.314	7.835
	5	3	0.378		24.61	25.55
^{53}Fe	7	1	0.000		34.88	39.42
^{54}Cr	4	6	0.835	−21(8)	−19.36	−23.25
^{54}Mn	6	4	0.000	+33(3)	31.41	35.16
^{54}Fe	4	2	1.408	−5(14)	−19.69	−20.40
	12	2	2.950		26.54	27.91
^{55}Mn	5	5	0.000	+33(1)	30.43	35.34
^{55}Fe	3	3	0.000		−12.41	−14.92
	5	3	0.931		−20.90	−24.73
	7	3	1.317		−23.53	−26.39
^{55}Co	7	1	0.000		25.22	26.44
^{56}Fe	4	4	0.847	−23(3)	−22.94	−27.33
^{56}Co	8	2	0.000	+25(9)	25.71	30.35
^{57}Co	7	3	0.000	+52(9)	30.82	36.72
	3	3	1.378		−17.81	−20.40
^{57}Ni	3	1	0.000		−4.571	−7.133
^{58}Co	4	4	0.000	+22(3)	18.47	21.30
	8	4	0.053		18.50	21.68
	6	4	0.111		26.84	34.47
^{58}Ni	4	2	1.454	−10(6)	−8.302	−12.41
^{58}Cu	2	0	0.000		5.446	6.334
^{59}Ni	3	3	0.000		1.444	2.014
	5	3	0.339		−9.713	−13.91
^{59}Cu	3	1	0.000		−13.25	−15.89
^{60}Ni	4	4	1.332	−10.4(18)	−10.07	−15.23
^{60}Cu	4	2	0.000		−6.702	−8.992
^{61}Ni	3	5	0.000	+16.2(15)	5.753	8.801
	5	5	0.067	−8(7)	−4.662	−6.731
				−20(3)		
^{62}Ni	4	6	1.173	+5(12)	6.057	8.525
^{63}Ni	5	7	0.087		1.1067	1.349
^{65}Ni	5	9	0.000		7.615	11.22

[a] From Ref. [21].

5. Conclusion

By considering a model space consisting of

$$0f_{7/2}^{n}(1p_{3/2}0f_{5/2}1p_{1/2})^{m} + 0f_{7/2}^{n-1}(1p_{3/2}0f_{5/2}1p_{1/2})^{1+m}$$

configurations, a study on a major part of the fp shell, i.e. the mass range $A = 41$–66, was carried out. By using the linear combination method an empirical interaction

was successfully obtained that can reliably describe various spectroscopic quantities for a wide range of nuclei in the mass range under consideration. The final interaction, denoted by TBLC8, where the 40 best-determined linear combinations out of a set of 177 parameters were allowed to vary, was obtained by fitting to a set of 494 level energies. It should be kept in mind that the results also depend on the starting interaction we adopted in order to fix the values of the matrix elements that are not well-determined by the data set. The final fit yielded an r.m.s. deviation of 193 keV between theoretical and experimental binding energies.

Good agreement was obtained with experimental values for the observables calculated with the TBLC8 wave functions, i.e. low-lying energy levels and static electromagnetic moments. In the next phase of this work extensive tests of the wave functions yielded by the new interactions are being performed, which includes the calculation of other observables such as spectroscopic factors, electromagnetic transition probabilities and Gamow–Teller strengths.

With the new TBLC8 interaction, some nuclei far from stability, i.e. the $N = 30$, 31 and 32 isotones, were also considered. The good results obtained for the energy spectra in this region supports the validity of the TBLC8 interaction far from the line of stability. It will also be interesting to extend the calculations to other nuclei far from stability.

The matrix elements of the TBLC8 interaction as well as a table of the fitted levels are available from the authors upon request.

Acknowledgement

W.R. wishes to ackonwledge the hospitality and support of the National Superconducting Cyclotron Laboratory, Michigan State University.

References

[1] W.A. Richter, M.G. van der Merwe, R.E. Julies and B.A. Brown, Nucl. Phys. A 523 (1991) 325.
[2] C.W. Johnson, S.E. Koonin, G.H. Lang and W.E. Ormand, Phys. Rev. Lett. 69 (1992) 3157.
[3] A.G.M. van Hees and P.W.M. Glaudemans, Z. Phys. A 303 (1981) 267.
[4] J.E. Koops and P.W.M. Glaudemans, Z. Phys. A 280 (1977) 181.
[5] M.G. van der Merwe, Ph.D. Thesis, University of Stellenbosch (1992).
[6] A. Etchegoyen, W.D.M. Rae, N.S. Godwin, W.A. Richter, C.H. Zimmerman, B.A. Brown, W.E. Ormand and J.S. Winfield, MSU-NSCL report (1985) 524.
[7] B.J. Cole, J. Phys. G. 11 (1985) 351.
[8] B.J. Cole, J. Phys. G 7 (1981) 173.
[9] M.W. Kirson, Phys. Lett. B 47 (1973) 110.
[10] K. Yoro, Nucl. Phys. A 333 (1980) 67.
[11] B.A. Brown, W.A. Richter, R.E. Julies and B.H. Wildenthal, Ann. Phys. 182 (1988) 191.
[12] B.H. Wildenthal, Prog. Part. Nucl. Phys. 11 (1984) 5.
[13] T.T.S. Kuo and G.E. Brown, Nucl. Phys. A 114 (1968) 241.
[14] W. Chung, Ph.D. Thesis, Michigan State University (1976).
[15] P.J. Brussaard and P.W.M. Glaudemans, Shell-model applications in nuclear spectroscopy (North-Holland, Amsterdam, 1977).
[16] H. Horie and K. Ogawa, Prog. Theor. Phys. 46 (1971) 439.

[17] H. Horie and K. Ogawa, Nucl. Phys. A 216 (1973) 407.
[18] A. Huck, G. Klotz, A. Knipper, C. Miehe, C. Richard-Serre, G. Walter, A. Poves, H.L. Ravn and G. Marguier, Phys. Rev. C 31 (1985) 2226.
[19] T. Motoba and K. Ogawa, Prog. Theor. Phys. 51 (1974) 173.
[20] P. Raghaven, At. Data Nucl. Data Tables 42 (1989) 189.
[21] T. Minamisono, S. Fukuda, T. Ohtsubo, A. Kitagawa, Y. Nakayama, Y. Someda, S. Takeda, M. Fukuda, K. Matsusa and Y. Nojiri, Nucl. Phys. A 559 (1993) 239.